Magnetic and superconducting instabilities in a hybrid model of itinerant/localized electrons for iron pnictides

Yi-Zhuang You,[1] Fan Yang,[2] Su-Peng Kou,[3] and Zheng-Yu Weng[1]

[1]*Institute for Advanced Study, Tsinghua University, Beijing, 100084, China*
[2]*Department of Physics, Beijing Institute of Technology, Beijing, 100081, China*
[3]*Institute for Advanced Study, Tsinghua University, Beijing, 100084, China*

We study a unified mechanism for spin-density-wave (SDW) and superconductivity in a minimal model in which itinerant electrons and local moments coexist as previously proposed for the iron pnictides [Kou, Li, Weng, EPL **88**, 17010 (2009)]. The phase diagram obtained at the mean-field level is in qualitative agreement with the experiment, which shows how the magnetic and superconducting (SC) instabilities are driven by the critical coupling between the itinerant/localized electrons. The spin and charge response functions at the random-phase-approximation level further characterize the dynamical evolution of the system. In particular, the dynamic spin susceptibility displays a Goldstone mode in the SDW phase, which evolves into a gapped resonance-like mode in the SC phase. The latter persists all the way into the normal state above T_c where a strong scattering between the itinerant electrons and local moments is restored, as an essential feature of the model.

I. INTRODUCTION

High-temperature superconductivity found[1,2] in the iron pnictides has attracted an intensive attention in recent years.[3] The superconducting (SC) pairing of the electrons in these materials is less likely to be mediated by phonons, as suggested by the local-density-approximation (LDA) calculations[4] as well as a variety of experiments.[3] The proximity of the SC state to the spin-density-wave (SDW) phase[5] in the phase diagram implies that the interplay between the magnetism and superconductivity might play an important role in understanding the pairing mechanism and other physical properties of the iron-based superconductors. Combined with the high SC transition temperature, one finds an intriguing resemblance between this family of materials and the cuprates in which superconductivity is generally believed to be of electronic origin.

Nevertheless, the electrons in the iron pnictides are more itinerant than those in the cuprates, especially in the magnetic phase, where the electrons in the latter are localized due to a Mott transition to form local moments, which become antiferromagnetically (AF) ordered at low temperature. By contrast, in the former, many different experiments have clearly demonstrated the itinerancy of the electrons in the SDW phase, including the multiple Fermi pockets as revealed by the angle-resolved photoemission spectroscopy (ARPES) measurements,[6–10] which are consistent with the LDA calculations,[11–15] the quantum-oscillation,[16] the transport[1,2,17] as well as the optical measurement.[18] Based on these experiments, one may reasonably view the magnetic order in this system as an SDW order formed by the itinerant electrons via Fermi-surface nesting.[13,15,19] From this point of view, it is natural to conjecture that the SC pairing is mediated by the collective magnetic fluctuations of the itinerant electrons. A lot of theoretical efforts have been done along this line, including the weak-coupling random-phase approximation (RPA) theory,[11,12,20,21] the fluctuation-exchange approximation (FLEX),[22,23] renormalization group (RG),[24] functional renormalization group (FRG),[25–27] and strong-

coupling variational Monte-Carlo (VMC)[28] approaches. The sign change in the gap function between the electron and hole pockets is predicted[11,12,25] as due to such unconventional magnetic origin of superconductivity.

However, the magnetism in the iron pnictides has been also looked upon from the strong-coupling side, where the electrons are localized via a multiband Mott transition forming local moments.[29–33] Indeed, the magnetic-ordering phase observed in experiment can be also described by utilizing a Heisenberg-type J_1-J_2 model.[34,35] A study of the SC state based on a doped Mott insulator described by the t-J_1-J_2 model also yields[36] a consistent pairing symmetry as compared to the experiment. This point of view is further supported by the first-principles LDA calculations, which generally show the tendency for a large magnetic moment formation at low doping.[37–41] A strong experimental support for the local moment picture comes from the observation of a linear temperature-dependent magnetic susceptibility in a broad temperature regime above the Néel temperature.[42–44] A recent neutron-scattering measurement[45] in $FeTe_{0.35}Se_{0.65}$ further observed a substantial magnetic moment persisting up to 300 K above T_c in the SC regime.

To reconcile the two aspects of the itinerant and localized electrons exhibited in the iron-based superconductors, a minimal model was proposed in Ref. 46, in which the itinerant electrons and the local moments are conjectured to coexist, based on the multiband nature of the system. Here, the two separated degrees of freedom may be attributed[47] to different $3d$ orbitals of the iron atoms, with the local moments formed via an orbital-selective Mott transition.[48] Recent dynamic mean-field theory (DMFT) calculations[49–51] lend numerical support for the possible orbital-selective Mott transition in the iron-based superconductors. Similar local-itinerant hybrid models incorporating the detailed orbital characters[52,53] have been used to account for the magnetic excitations observed in the iron pnictides.

The most essential feature in the model of coexistent itinerant/localized electrons lies in the momentum match between the two degrees of freedom.[46] Namely, the

characteristic wave vector of the magnetic correlation of the local moments, $\mathbf{Q}_s = (\pi,0)$ or $(0,\pi)$, is commensurate with the typical momentum transfer between the hole and electron pockets of the itinerant electrons. Consequently, the scattering between the two degrees of freedom, which are coupled by the Hund's rule interaction, can get much enhanced in the normal state, rendering the system intrinsically unstable toward either the magnetic or SC ordering at low temperatures. At low doping, the magnetically ordered state can be obtained[46] as composed of an SDW order of the itinerant electrons simultaneously locking with the collinear magnetic order of the local moments at the same wave vector $\mathbf{Q}_s$. Here, the nesting effect in the itinerant degrees of freedom alone or a pure J_1-J_2 superexchange interaction in the local moment part can be much weaker themselves in driving the magnetic transition. For example, a perfect nesting of the Fermi surfaces can be easily removed by adjusting the chemical potential[46] or by introducing a more realistic band structure.[52] The pure collinear AF ordering for the local moments can be also switched off by setting[46] $J_1 = 0$ and (or) making the subsystem in the disordered regime. But the hybrid system can nevertheless experience an SDW phase transition due to the magnetic instability driven by the above-mentioned critical coupling between the two subsystems. The residual scattering between the itinerant and localized electrons will become much reduced in the SDW state, which exhibits[46,52] a series of magnetic and charge properties qualitatively consistent with the iron-based superconductors at low doping.

However, the SDW instability studied in Ref. 46 is only one of the possible infrared fixed points of this minimal model at low doping. In this paper, we shall show that another instability in which the itinerant electrons become Cooper paired can happen at higher doping to compete with the SDW state. By opening up SC gaps at the Fermi surfaces of the hole and electron pockets, the system can also be stabilized in reducing the residual scattering between the itinerant and localized electrons. We obtain a global phase diagram for the SDW and SC states at the mean-field level on equal footing, which is in qualitative consistency with the experimental ones for the iron-based superconductors. We further go beyond the mean-field approximation to study the spin dynamics at the RPA level. In the SDW state, the magnetic excitation is predicted to split into two branches, composed of a low-lying Goldstone mode and a gapped high-energy mode dominantly contributed by the local moments. The latter generally gets severely broadened due to the strong scattering between the itinerant electrons and local moments. In the SC state, such a Goldstone mode is then replaced by a low-lying gapped resonance-like mode, which can persist all the way to the high-temperature normal state, consistent with the neutron-scattering observations.[57] The band renormalization as well as the charge scattering in the transport channel are also studied within the same framework. The results in this model study will illustrate a phenomenology consistent with the iron-based superconductors in which neither the Fermi-surface nesting for the itinerant electrons nor the superexchange interaction for the local moments play the direct role alone. Rather these effects get strongly enhanced via the Hund's rule coupling between the two subsystems with the momentum match. The

latter effect makes the system generically unstable against the SDW/SC orderings at different doping and therefore provides a unified mechanism to understand both orders appearing in the iron pnictides.

The remaining part of the paper is organized as follows. In Sec. II, we introduce the basic model, which includes a two-pocket description of the itinerant electrons and a nonlinear σ-model description of the local moments, which are coupled together by the Hund's rule coupling. In Sec. III, we present a mean-field calculation, which gives rise to a global phase diagram with both the SDW and SC orders identified at different dopings. Section IV is on the dynamic fluctuation beyond the mean-field approximation, including the RPA calculations of the dynamic spin susceptibility, the uniform magnetic susceptibility in different phases, and the band renormalization effect. Finally, the conclusions and discussion are presented in Sec. V.

II. MODEL DESCRIPTION

Our starting point is an itinerant-electron and local-moment hybrid model, previously proposed[46] to describe the iron-based superconductors. We shall explore the emergent magnetism and superconductivity in this highly simplified model, which is to be specified below.

A. Model action

The effective action includes an itinerant-electron sector S_{it}, a local-moment sector S_{loc}, and a Hund's rule coupling term S_{H} as follows

$$S_{\text{eff}} = S_{\text{it}} + S_{\text{loc}} + S_{\text{H}}. \tag{1}$$

1. Itinerant electron

We consider a simple two-pocket model for the itinerant electrons, whose action reads

$$S_{\text{it}} = \sum_k c_k^\dagger (-i\omega + \xi_{\boldsymbol{k}}) c_k, \tag{2}$$

where $k = (i\omega, \boldsymbol{k})$ is the (fermionic) momentum-frequency vector and $c^\dagger = (c_{\Gamma\uparrow}^\dagger, c_{\Gamma\downarrow}^\dagger, c_{M\uparrow}^\dagger, c_{M\downarrow}^\dagger)$ contains the creation operators of the itinerant electron for both spins ($\uparrow$ and $\downarrow$) and in the hole and electron pockets denoted by Γ and M, respectively (see below). The momentum-frequency summation stands for $\sum_k = \beta^{-1} \sum_{i\omega} \sum_{\boldsymbol{k}}$, where $\beta^{-1} = k_B T$, and this convention will be adopted throughout this work.

Matrix $\xi_{\boldsymbol{k}}$ is a 4×4 and determines the band dispersion. It may be written as

$$\xi_{\boldsymbol{k}} = -\mu\rho_0 - \epsilon_{\boldsymbol{k}}\rho_3, \tag{3}$$

where $\rho_i \equiv \sigma_i \otimes \sigma_0$ is the 4×4 matrix defined by the Kronecker product of the Pauli matrices σ_i (where σ_0 is the identity 2×2 matrix), μ is the chemical potential, and $\epsilon_{\boldsymbol{k}} = \boldsymbol{k}^2/(2m) - \epsilon_0$ models a parabolic band dispersion with the effective mass m and the energy shift ϵ_0.

According to ARPES,[6–9] magneto-oscillation experiments,[16] and LDA calculations,[11–15] both Fermi pockets are small (with $k_F \sim \pi/10$) and shallow ($E_F \sim 0.1$ eV). So by
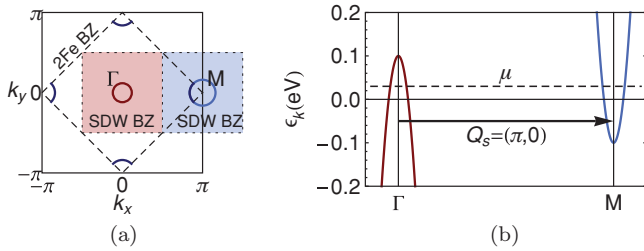
FIG. 1. (Color online) (a) The Fermi surface consists of a small hole pocket around the Γ point and a small electron pocket around M. Both pockets locate around the origin in the SDW Brillouin zone. (b) Band structure. The nesting vector $\boldsymbol{Q}_s = (\pi,0)$ connects the two bands.
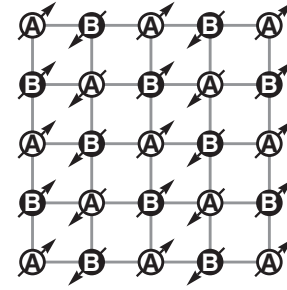

FIG. 2. Each circle in the figure represents a Fe atom. The Fe lattice is divided in to A and B sublattices. In each set of the lattice, the local moments interact by the nearest AF coupling (next nearest in the original lattice).

setting the parameters at $m = 0.1$ eV^{-1} and $\epsilon_0 = 0.1$ eV, we can produce a reasonable band structure as shown in Fig. 1.

There are several aspects that we wish to comment on this simple two-pocket model. Firstly, at $\mu = 0$, the hole and the electron Fermi pockets perfectly match under a momentum translation $\boldsymbol{Q}_s = (\pi,0)$. In real materials, the nesting is not perfect even in the undoped case,[6–9,11–15] which may represented by a small but finite $|\mu|$ here. Secondly, the detailed orbital characters are neglected with the pockets taken to be rotationally symmetric. Such a simple model can not account for some anisotropic phenomenon such as the nodal SDW gap as discussed in Ref. 54. Thirdly, for simplicity in the present two-pocket band structure, we focus on the electron pocket around $(\pi,0)$ point and the hole pocket around $(0,0)$, which are connected by $\boldsymbol{Q}_s = (\pi,0)$, because in the SDW phase only one of the electron pockets, together with the Γ pocket, will mainly contribute to the SDW ordering. For the sake of simplicity, the same simplified model is used in studying the SC phase, where, in general, both electron pockets should participate in pairing, which would enhance superconductivity but should not qualitatively change the main results obtained in this work.

2. Local moment

For local moments, we simply consider an AF superexchange coupling J_2 bridged by the As ions between the diagonal Fe sites. Although in general, the nearest-neighboring coupling J_1 may be present as well, which helps to lock the spins into the collinear AF order, however, by coupling to the hole and electron pockets, it is found that the itinerant electrons may play the same role as J_1 to drive the system to a collinear AF order. In this sense, the bare J_1 term is not very essential.

The local moments at the Fe sites may be divided into two sets of sublattices, each is described by an AF Heisenberg model. The effective Hamiltonian may be written as

$$H_{\text{loc}} = J_2 \sum_{X=A,B} \sum_{\langle rr' \rangle \in X} \boldsymbol{M}_r \cdot \boldsymbol{M}_{r'}, \qquad (4)$$

where $X = A, B$ labels the sites on different sublattices as shown in Fig. 2, and $\langle rr' \rangle$ denotes the nearest-neighboring sites in the same sublattice (or equivalently the next-nearest-neighboring sites in the original lattice).

The local moment $\boldsymbol{M}_r$ will intrinsically fluctuate around the characteristic momentum $\boldsymbol{Q}_s = (\pi,0)$ or $(0,\pi)$. So we may

take $\boldsymbol{M}_r = M n_r e^{i \boldsymbol{Q}_s \cdot r}$ with n_r a unit three-component real vector field such that n_r fluctuates smoothly in the space, which will be convenient for further field theoretical treatments.

The low-energy AF fluctuation of the local moment in each sublattice may be described by a nonlinear σ model. The corresponding action reads $S_{\text{loc}} = \sum_{X=A,B} S_X$, with

$$S_X = \frac{1}{4g} \sum_q n_{X,-q}(\nu^2 + c^2 \boldsymbol{q}^2 + \eta^2) n_{X,q} - \frac{\eta^2}{4g}, \qquad (5)$$

where $q = (i\nu, \boldsymbol{q})$ denotes the (bosonic) momentum-frequency vector and $n_{X,q} = \int_0^\beta d\tau \sum_{r \in X} e^{i(\boldsymbol{q}\cdot\boldsymbol{r} - \nu\tau)} n_r(\tau)$ is Fourier transformed from the field n_r in the X sublattice. Entity η^2 is the Lagrangian multiplier that enforces the unit condition $n_r^2 = 1$. According to the above definition, a long-wavelength limit at $\boldsymbol{q} \to 0$ actually corresponds to the real momentum $\to \boldsymbol{Q}_s$.

The coupling constant g and spin-wave velocity c are related to the Heisenberg J_2-model by $g = 8J_2$ and $c = 4J_2 M$ (with the Fe-Fe distance taken as the unit).[46] From the neutron-scattering experiments,[34] the typical spin-wave velocity is around 0.3 eV, so that we set $c = 0.3$ eV, which in turn determines $J_2 = 0.093$ eV and $g = 0.75$ eV, assuming the magnetic moment $M = 0.8$ per Fe atom.

By introducing a parallel field $n = (n_A + n_B)/2$ and an antiparallel field $\tilde{n} = (n_A - n_B)/2$, the action can be further written as

$$S_{\text{loc}} = \frac{1}{2g} \sum_q n_{-q}(\nu^2 + c^2 \boldsymbol{q}^2 + \eta^2) n_q$$
$$+ \frac{1}{2g} \sum_q \tilde{n}_{-q}(\nu^2 + c^2 \boldsymbol{q}^2 + \eta^2) \tilde{n}_q - \frac{\eta^2}{2g}. \qquad (6)$$

3. Coupling term

The itinerant electron spin $\boldsymbol{S}_r = S c_r^\dagger \sigma c_r$ at site r can be coupled to the local moment $\boldsymbol{M}_r$ at the same site by a Hund's rule interaction

$$H_{\text{cp}} = -J_H \sum_r \boldsymbol{M}_r \cdot \boldsymbol{S}_r, \qquad (7)$$

where J_H denotes the strength of the effective Hund's rule coupling. Fourier transformation to the momentum-frequency space yields the following action

$$S_{cp} = -J_0 \sum_{k,q} n_q \cdot c^\dagger_{k+q} s c_k, \qquad (8)$$

where $J_0 \equiv 2J_H M S$, M is the magnitude of the local moment and $S = 1/2$ for the itinerant electron. In Eq. (8), $s \equiv (s_1, s_2, s_3)$ with each s_i ($i = 1,2,3$) as a 4×4 matrix defined by $s_i \equiv \sigma_1 \otimes \sigma_i$.

The itinerant electrons will couple to the parallel field n, which mainly causes the scattering between the Γ pocket and the M pocket at $(\pi,0)$, and to the antiparallel field $\tilde{n}$, which mainly causes the scattering between the Γ and $(0,\pi)$ pockets.

B. Mass-gap equation

To simplify the calculation, we replace the Lagrangian multiplier η^2 by its saddle point value. Evaluating the saddle point equation $\delta S_{loc}/\delta(\eta^2) = 0$ at the one-loop level yields

$$-\frac{1}{2g}\left(1 - n_0^2\right) + 3\sum_q \frac{1}{v_n^2 + c^2 q^2 + \eta^2} = 0, \qquad (9)$$

where $n_0 \equiv \langle n_{q=0} \rangle$ denotes the mean-field value of the local moment.

Carrying out the momentum and frequency summations, η can be solved from the above equation as follows

$$\eta = \eta_0 + \frac{2}{\beta} \ln \frac{1}{2}(1 + \sqrt{1 + 4e^{-\beta\eta_0}}), \qquad (10)$$

where η_0 is the solution of η at zero temperature, which reads

$$\eta_0 = \frac{2\pi c^2}{3g_c} \frac{1 - \gamma^2}{2\gamma}, \qquad (11)$$

where $\gamma = (g_c/g)(1 - n_0^2)$. The parameter $g_c = 2\pi c/(3\Lambda)$ is introduced to replace the momentum cutoff Λ, which is needed to control the convergence of the momentum summation.

The physical meaning of η is the mass gap of the bare spin-wave excitation in the local-moment sector. If $g > g_c$, the mass gap will remain finite at zero temperature, indicating a disordered state with only short-range magnetic ordering for the pure local-moment degrees of freedom. We shall see that due to the strong coupling between the itinerant electrons and local moments, a true SDW order can be still induced, even if the bare local moments are in a disordered regime and do not order at $T = 0$ by themselves.

C. Propagators

The itinerant electron single-particle propagator is denoted by $G(k) \equiv -\langle c_k c^\dagger_k \rangle$, and represented by the arrowed line ⟵ in the Feynman diagram. Matrix $G(k)$ is 4×4 since $c^\dagger_k$ has 4 components (2 pockets × 2 spins). The propagator for the local moment is denoted by $D(q) \equiv -\langle n_{-q} n_q \rangle$, and represented by the dashed line ┅┅ in the Feynman diagram. Matrix $D(q)$ is 3×3 because n_q has 3 components.

The double lines in the Feynman diagram represent the dressed propagators, while the single lines, such as ⟵ and ┅┅, denote the bare propagators G_0 and D_0, respectively.

The latter can be read out directly from the actions S_{it} and S_{loc} as

$$G_0(k) = (i\omega - \xi_k)^{-1} = \frac{(i\omega + \mu)\rho_0 - \epsilon_k \rho_3}{(i\omega + \mu)^2 - \epsilon_k^2} \qquad (12)$$

and

$$D_{0,ii'}(q) = \frac{-g\delta_{ii'}}{v^2 + c^2 q^2 + \eta^2}. \qquad (13)$$

III. MEAN-FIELD PHASE DIAGRAM

In the effective action Eq. (1), even though the two subsystems, i.e., the local moments and itinerant electrons, may not be in a magnetic or SC ground state separately, the whole system coupled together will experience intrinsic magnetic and SC instabilities, which are studied on equal footing below at the mean-field level.

A. SDW phase

The SDW mean-field equation can be deduced from the following Dyson equation for the self-consistent Hartree approximation

$$\qquad (14)$$

or

$$G(k) = G_0(k) + G_0(k)\Sigma_d G(k), \qquad (15)$$

where the Hartree self-energy is given by

$$\Sigma_d = J_0^2 D_{0,ii'}(q = 0)s_i \sum_{k'} \text{Tr}[G(k')s_{i'}]. \qquad (16)$$

On the other hand, the Hartree energy is related to the local-moment mean field by

$$\Sigma_d = -J_0 n_{0i} s_i, \qquad (17)$$

where n_{0i} is the ith component of $\langle n_{q=0} \rangle$. This can be seen by separating out the $q = 0$ term $-J_0 \sum_k n_0 \cdot c^\dagger_k s c_k$ from the summation in the coupling term in Eq. (8). This term indicates that the local-moment mean field n_0 affects the itinerant electron Hamiltonian by adding the self-energy $-J_0 n_0 \cdot s$, which should just be identified as the Hartree energy. The consistency between Eqs. (16) and (17) leads to the SDW mean-field equation. To show this, we first take Eq. (17) and evaluate the propagator from Eq. (15):

$$G(k) = \frac{(i\omega + \mu)\rho_0 - \epsilon_k \rho_3 - J_0 n_{0i} s_i}{(i\omega + \mu)^2 - \epsilon_k^2 - J_0^2 n_0^2}. \qquad (18)$$

Substituting into Eq. (16) yields

$$\Sigma_d = \frac{4g J_0^3 n_{0i} s_i}{\eta^2} \sum_k \frac{1}{(i\omega + \mu)^2 - \epsilon_k^2 - J_0^2 n_0^2}. \qquad (19)$$

After Matsubara frequency summation, we have

$$\Sigma_d = -\frac{4g J_0^3 n_{0i} s_i}{\eta^2} \sum_k \frac{\sinh \beta E_k}{2E_k(\cosh \beta \mu + \cosh \beta E_k)}, \qquad (20)$$

where $E_{\bm{k}}^2 = \epsilon_{\bm{k}}^2 + J_0^2 n_0^2$. Comparing with Eq. (17), we arrive at the SDW mean-field equation,

$$\frac{4g J_0^2}{\eta^2} \sum_{\bm{k}} \frac{\sinh \beta E_{\bm{k}}}{2 E_{\bm{k}} (\cosh \beta \mu + \cosh \beta E_{\bm{k}})} = 1, \qquad (21)$$

from which the SDW order parameter n_0 can be determined for the given chemical potential and temperature.

B. SC phase

To deal with the SC order, we introduce the abnormal propagator for the itinerant electrons: $F(k) \equiv -\langle c_k c_{-k} \rangle$, represented by a line with two arrows heading in opposite directions $\Longleftrightarrow$.

The SC mean-field equations are equivalent to the following Dyson equations of self-consistent Fock approximation,[55]

$$(22)$$

The above diagrams correspond to

$$\begin{aligned} G(k) &= G_0(k) - G_0(k) \Sigma_p(k) F(-k), \\ -F(k) &= G_0(k) \Sigma_p(k) G(-k), \end{aligned} \qquad (23)$$

where the pairing energy is

$$\Sigma_p(k) = -J_0^2 \sum_{k'} D_{0,ii'}(k - k') s_i F(k') \left(-s_{i'}^{\mathsf{T}} \right). \qquad (24)$$

Mediated by the local-moment fluctuation, the effective interaction between the itinerant electrons is described by the following action:

$$S_{\text{int}} = \sum_{k,k',p} c_{k+p}^\dagger c_{-k}^\dagger \Gamma(k - k') c_{-k'} c_{k'+p}, \qquad (25)$$

where the vertex function reads

$$\Gamma(q) = - \begin{array}{c} \bullet \\ \bullet \end{array} = \frac{J_0^2}{2} D_{0,ii'}(q) s_i \otimes s_{i'}. \qquad (26)$$

The eigenvalue of the kernel function $\Gamma(k - k')$ stands for the effective pairing energy of the Cooper pair, whose form factor is given by the corresponding eigenvector. The most negative eigenvalue (hence the strongest pairing attraction) is found in the spin-singlet intra-pocket pairing channel with $s^\pm$-wave symmetry. In fact, simply by diagonalizing the matrix $s_i \otimes s_i$, it is easy to show that the greatest eigenvalues belong to the spin-singlet parings with opposite sign between the electron and the hole pocket. Among the spin-singlet pairing channels, the interpocket pairing would lead to the pocket singlet, which requires the gap function to be of p-wave symmetry and is not able to fully gap the Fermi surface, and thus the intrapocket $s^\pm$-wave pairing remains most favorable.

By introducing a 4×4 matrix $d^\dagger \equiv \sigma_3 \otimes (i \sigma_2)$, the $s^\pm$-wave paring operator can be simply denoted as

$$\begin{aligned} c_k^\dagger d^\dagger c_{-k}^\dagger &= \left(c_{k\Gamma\uparrow}^\dagger c_{-k\Gamma\downarrow}^\dagger - c_{k\Gamma\downarrow}^\dagger c_{-k\Gamma\uparrow}^\dagger \right) \\ &\quad - \left(c_{kM\uparrow}^\dagger c_{-kM\downarrow}^\dagger - c_{kM\downarrow}^\dagger c_{-kM\uparrow}^\dagger \right). \end{aligned} \qquad (27)$$

Therefore, one may assume the pairing energy to take the same form

$$\Sigma_p(k) = \Delta(k) d, \qquad (28)$$

with symmetric gap function $\Delta(k)$, i.e., $\Delta(-k) = \Delta(k)$. Although the other pairing modes may also appear in Σ_p, they are all omitted to simplify the derivation. In general, an s^{++}-wave pairing can be also induced from $s^\pm$-wave pairing if the two Fermi pockets are no longer symmetric in size (i.e., with a finite chemical potential μ in our model). However, according to our calculation, the $s^\pm$-wave will be the dominant component persisting up to larger μ.

Then from Eq. (23), one can find the solution of $G(k)$ and $F(k)$,

$$G(k) = \frac{Z(k) \rho_0 - E(k) \rho_3}{Z(k)^2 - E(k)^2}, \qquad (29)$$

where

$$\begin{aligned} Z(k) &= \frac{(i\omega - \mu)^2 - \epsilon_{\bm{k}}^2 - \Delta(k)^2}{(i\omega - \mu)^2 - \epsilon_{\bm{k}}^2} (i\omega - \mu) + 2\mu, \\ E(k) &= \frac{(i\omega - \mu)^2 - \epsilon_{\bm{k}}^2 - \Delta(k)^2}{(i\omega - \mu)^2 - \epsilon_{\bm{k}}^2} \epsilon_{\bm{k}}, \end{aligned} \qquad (30)$$

and

$$F(k) = f(k) \Delta(k) d, \qquad (31)$$

where

$$f(k) = \frac{1}{2} \sum_{\varsigma = \pm 1} \frac{1}{(i\omega)^2 - (\epsilon_{\bm{k}} + \varsigma \mu)^2 - \Delta(k)^2}. \qquad (32)$$

Here, we have projected out the components other than $s^\pm$-wave in the solution of $F(k)$ as noted above. Substituting the above solutions into Eq. (24) yields

$$\Sigma_p(k) = 3 J_0^2 \sum_{k'} D_{0,11}(k - k') f(k') \Delta(k') d. \qquad (33)$$

Comparing with Eq. (28), we arrive at the SC mean-field equation

$$\Delta(k) = 3 J_0^2 \sum_{k'} D_{0,11}(k - k') f(k') \Delta(k'). \qquad (34)$$

This equation can be solved by a numerical approach.

To proceed with analytic analysis, we omit the k dependence of $\Delta(k)$ and replace it by a constant Δ. We also approximate $D_0(k - k')$ by its average value $\langle D_0 \rangle$ at zero frequency around the Fermi surface,

$$\langle D_0 \rangle = -g \left\langle \frac{1}{c^2 (\bm{k} - \bm{k}')^2 + \eta^2} \right\rangle_{k,k' \in \text{FS}} = -\frac{g}{\eta_{\text{eff}}^2}. \qquad (35)$$

One finds $\eta_{\text{eff}}^2 = \eta (\eta^2 + 4 c^2 k_F^2)^{1/2}$ with $k_F^2 = 2 m \epsilon_0$. Then the SC mean-field equation becomes

$$1 = -\frac{3g J_0^2}{\eta_{\text{eff}}^2} \sum_{k} f(k), \qquad (36)$$

which, after the Matsubara frequency summation, yields

$$1 = \frac{3g J_0^2}{2 \eta_{\text{eff}}^2} \sum_{\varsigma = \pm 1} \sum_{k} \frac{1}{2 E_{\varsigma, k}} \tanh \frac{\beta E_{\varsigma, k}}{2}, \qquad (37)$$

where $E_{\varsigma, \bm{k}}^2 = (\epsilon_{\bm{k}} + \varsigma \mu)^2 + \Delta^2$, which determines the SC gap Δ.
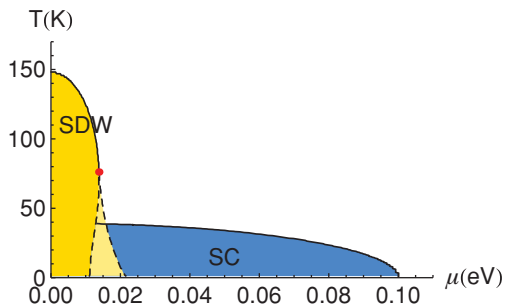
FIG. 3. (Color online) The phase diagram calculated according to the mean-field equations. The solid lines denote the second-order phase transition boundaries and the dashed lines denote the first-order phase transition boundaries. The red point is a critical point. The SDW and SC phase boundaries are calculated independently, and the overlap region does not necessarily imply the coexistence of two orders.
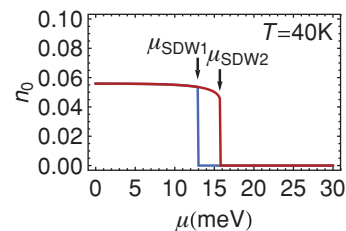

FIG. 4. The SDW order as a function of chemical potential at $T = 40$ K, showing the hysteresis loop of the first ordered transition with two distinct transition chemical potentials.

C. Phase diagram

By solving self-consistently the two mean-field equations, Eqs. (21) and (37), the phase diagram of the SDW and SC phases can be determined as shown in Fig. 3. In the following, we specify the choice of the parameters in the model.

It is noted that there are three particular points in the phase diagram that can be calculated analytically based on the mean-field equations. They are the SDW critical temperature T_{SDW}^0 at $\mu = 0$, the SC critical temperature T_c^0 at $\mu = 0$ (if not consider SDW), and the chemical potential μ_{SDW1} at which the SDW order disappears at zero temperature. The formulas read

$$T_{SDW}^0 = 1.13 T_0 e^{-1/(N_F^0 V_{SDW})}, \tag{38}$$

$$T_c^0 = 1.13 T_0 e^{-1/(N_F^0 V_{SC})}, \tag{39}$$

and

$$\mu_{SDW1} = T_0 e^{-1/(N_F^0 V_{SDW})}, \tag{40}$$

where $N_F^0 = m/(2\pi)$ is the density of states at the Fermi energy $\mu = 0$, $T_0 \equiv \epsilon_0 (\Lambda^2/(2m\epsilon_0) - 1)^{1/2}$, $V_{SDW} = 4g J_0^2/\eta^2$, and $V_{SC} = 3g J_0^2/\eta_{eff}^2$. To be overall comparable to the experiments, we take $T_{SDW}^0 \simeq 150$ K and $T_c^0 \simeq 40$ K and, making use of Eqs. (38) and (39) to fix the model parameters, $g_c = 0.53$ eV and $J_0 = 0.39$ eV. Consequently, with all the basic parameters in our model given, the phase diagram is determined numerically as a function of the chemical potential in Fig. 3.

Figure 3 shows a critical point at the SDW phase boundary, located at $\mu^* = 0.014$ eV and $T^* = 76$ K, where the second-order phase-transition boundary splits into two first-order phase-transition boundary lines. Hence, at $T = 0$, there exist two critical chemical potentials for the SDW transition: $\mu_{SDW1} = 0.011$ eV and $\mu_{SDW2} = 0.022$ eV, respectively, as shown in Fig. 4. A similar first-order transition phenomenon has been also reported[56] in another theoretical approach based on a pure itinerant model.

Figure 3 shows that the SC critical temperature is not sensitive to the chemical potential, in contrast to the SDW state, because the pairing mechanism of the present model is not sensitive to the Fermi-surface nesting condition. On the other hand, the $s^{\pm}$-wave superconductivity does require finite Fermi-surface densities of states in both hole and electron pockets to support the intrapocket pairing. That explains why T_c eventually vanishes at $\mu = 0.1$ eV when the Fermi level touches one of the band bottoms of the hole/electron pockets. It is noted that beyond $\mu = 0.1$ eV, superconductivity of other types of pairing symmetry is still possible in the present model, which will involve the intra-electron or hole-pocket pairing and require some incommensurate AF fluctuations of the local moment away from $\mathbf{Q}_s$.

Therefore, the high-temperature normal state can be regarded as an unstable fixed-point state in the present model in which the itinerant electrons scatter strongly with the local moments due to the momentum match at $\mathbf{Q}_s$ and the model defines the relevant degrees of freedom that render the system flow into either an SDW or SC ordered phase, depending on doping, as the temperature lowers. The mean-field Eqs. (21) and (37) describe, respectively, how the SDW and SC orders emerge from such a normal state, with the phase diagram in qualitative agreement with the iron superconductors.[3]

Finally, we point out that although Fig. 3 suggests that the SDW and SC phases may coexist at low doping, in mapping out the phase diagram in the figure, only the maximal temperature of T_{SDW} and T_c are shown at a given μ with the assumption that the other order in the mean-field equations vanishes. In other words, in order to determine the coexistent SC state *inside* the SDW regime, one needs to further incorporate the detailed competition of the two orders into the self-consistent mean-field equations, which can be straightforwardly done by generalizing the above formulation. But this is not considered here not only for the sake of simplicity, but also because we wish to emphasize that the mutual interplay between the SDW and SC orders is *not* essential in driving their own formations in our model.

IV. DYNAMIC FLUCTUATIONS

The interaction between the itinerant and localized electrons has played a crucial role in resulting in the SDW and SC states, as described by the global diagram in Fig. 3. In the following, we further investigate the evolution of dynamic fluctuations beyond the mean-field approximation in these phases.

A. Dynamic spin susceptibility

To study the low-energy spin dynamics around the SDW wave vector $\mathbf{Q}_s$, we first consider the RPA correction to the propagator $D(q)$ of the local moment by the Dyson equation

$$\text{===} = \text{----} + \text{----}\bigcirc\text{===}, \tag{41}$$

or

$$D(q) = D_0(q) + D_0(q)\Pi(q)D(q), \tag{42}$$

which is solved formally as

$$D(q) = \frac{D_0(q)}{1 - D_0(q)\Pi(q)}, \tag{43}$$

where the RPA bubble Π is given by

$$\Pi_{ii'}(q) = -\bigcirc = J_0^2 \sum_k \text{Tr}\left[s_i G(k)s_{i'}G(k+q)\right]. \tag{44}$$

Here, as the propagator of the itinerant electron, the particular form of $G(k)$ depends on the mean-field states; in the normal state, it takes the form of Eq. (12) and in the SDW state, it is given by Eq. (18). While in the SC state, the contribution from the abnormal propagator should be included as well

$$
\begin{aligned}
\Pi_{ii'}(q) = &-\bigcirc - \bigcirc \\
= &J_0^2 \sum_k \text{Tr}\left[s_i G(k)s_{i'}G(k+q)\right] \\
&+ J_0^2 \sum_k \text{Tr}\left[s_i F(k)(-s_{i'}^{\mathsf{T}})F^\dagger(k+q)\right],
\end{aligned} \tag{45}
$$

where Eqs. (29) and (31) are used.

By noting that $-J_0^{-2}\Pi(q)$ represents the spin susceptibility of the itinerant electrons at the mean-field level, one can similarly write down the spin susceptibility of the itinerant electrons at the RPA level, and finally obtain the following total spin susceptibility

$$\chi(q) = -\frac{D_0(q) + J_0^{-2}\Pi(q)}{1 - D_0(q)\Pi(q)}. \tag{46}$$

The inelastic neutron-scattering spectroscopy (INS) can measure the dynamic spin susceptibility as the imaginary part of $\chi(q)$, $-\text{Im}\chi(\nu + i0_+, \mathbf{q})$, obtained after the Wick rotation $i\nu \to \nu + i0_+$, which is presented in Fig. 5 in different phases (see the figure caption for the details).

In the normal state, as Fig. 5(a) shows, the spectrum of the local-moment fluctuation becomes very fuzzy when it immerses into the continuum of the itinerant electrons as indicated by the dome-shaped shadow area around $q \lesssim 0.2$. For comparison, the bare dispersion of the local-moment spin wave is marked out by the dashed curve (which is gapped as in a disordered regime of the nonlinear σ model as noted before). The smearing of the spectrum is clearly the result of the strong scattering between the itinerant and local moment in the region around $\mathbf{Q}_s$. At $q \simeq 0$, a hot spot at the frequency slightly below 2μ can be seen in Fig. 5(a). This is because the creation of a spin flip at $q = 0$ involves a pair of electron and hole excitations at the Γ and M pockets, respectively, which
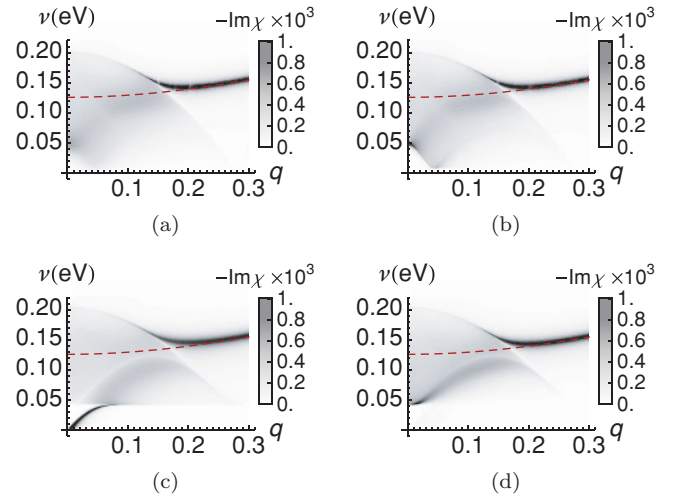

FIG. 5. (Color online) The calculated spectral function of dynamic spin susceptibility. Darker shade indicates higher intensity: (a) in the normal phase ($\mu = 0.03$ eV and $T = 50$ K), (b) in the SC phase ($\mu = 0.03$ eV and $T = 30$ K), and (c) and (d) are both in the SDW phase ($\mu = 0.00$ eV and $T = 80$ K) snowing the spectrum of transverse and longitudinal fluctuations, respectively. The red dashed curve marks out the bare spin-wave dispersion.

costs at least energy 2μ to go across the Fermi surface, and on the other hand, the gap of the local-moment fluctuation is higher than this energy such that the scattering diminishes. As a matter of fact, such a resonance-like mode becomes even sharper in the SC phase [see Fig. 5(b)] simply due to the further reduction of the scattering with the opening of the SC gap. It may account for the resonance mode found in the INS experiment,[57] which indeed persists all the way to the normal state.

In the SDW state at low doping, inside the SDW gap of the itinerant electrons, the fuzzy continuum is replaced by some emergent collective modes. The transverse spin fluctuations (in the directions perpendicular to the ordering direction) become the gapless Goldstone modes [see Fig. 5(c)], which is consistent with the previous RPA calculation using a more complicated five-band model for the itinerant electrons.[52] On the other hand, the longitudinal fluctuation (along the ordering direction) remains gapped as shown in Fig. 5(d).

The existence of the Goldstone mode can be proven rigorously at the RPA level. Since the RPA bubble in the SDW phase has a rather simple expression at zero frequency and momentum,

$$\Pi_{ii'}(0) = -4J_0^2 \sum_k \left(\delta_{ii'} - \frac{J_0^2 n_{0i}n_{0i'}}{E_k^2}\right)$$

$$\times \frac{\sinh\beta E_k}{2E_k(\cosh\beta\mu + \cosh\beta E_k)}. \tag{47}$$

Let us suppose that the SDW ordering is along the third direction in the spin space, i.e., $n_{0,1} = n_{0,2} = 0$ and $n_{0,3} \neq 0$. Then $\Pi_{11}(0) = \Pi_{22}(0) \leqslant \Pi_{33}(0) < 0$, and by comparing with Eq. (20) and referring to Eq. (13), it is recognized that

$$\Sigma_d = \frac{g J_0 n_{0i} s_i}{\eta^2}\Pi_{11}(0) = -J_0 n_{0i}s_i D_{0,11}(0)\Pi_{11}(0). \tag{48}$$
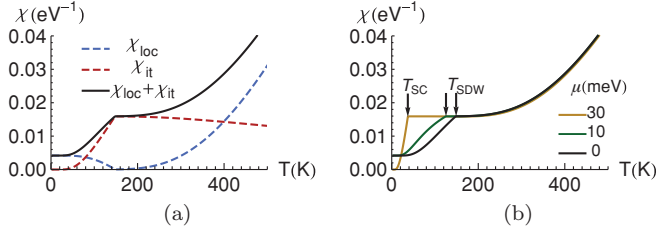
FIG. 6. (Color online) (a) The uniform susceptibility vs temperature at $\mu = 0$. The dashed lines indicate the contributions from either the local moment (blue) or the itinerant electron (red). The solid line is the total uniform susceptibility. (b) The total uniform susceptibility curves at various chemical potentials μ, all show a rapid drop in the ordered phase at low temperature.

As the self-energy Σ_d is determined self-consistently from the SDW mean-field equation $\Sigma_d = -J_0 n_{0i} s_i$, at the mean-field saddle point, we have $D_{0,11}(0)\Pi_{11}(0) = 1$, which leads to a pole of D_{11} at $q = 0$ according to $D = (1 - D_0\Pi)^{-1}D_0$, proving the existence of a zero-energy collective mode, i.e., the Goldstone mode. The same argument applies for the D_{22} component as well. Also taken into account the fact that $D_{12} = 0$, it can be concluded that there are two Goldstone modes, both are in the transverse directions. As for the D_{33} component, since $\Pi_{33} \geqslant \Pi_{11}$ such that $D_{0,33}(0)\Pi_{33}(0) \leqslant 1$ [note that $D_0(0)$ is negative], no pole can appear at $q = 0$ in general, meaning that the longitudinal mode is still gapped.

B. Uniform susceptibility

The total uniform susceptibility $\chi = \chi_{\text{loc}} + \chi_{\text{it}}$ at $\mu = 0$ is presented in Fig. 6(a) in which the contributions from both the local moment and the itinerant electron degrees of freedom, i.e., χ_{loc} and χ_{it}, respectively, are also given. In Fig. 6(b), the uniform susceptibility is shown at different μ's where the low-temperature phases are either SDW or SC.

To probe the uniform susceptibility for the local moment, we add a Zeeman term $-M\sum_i h\,n_i$ to the local-moment Hamiltonian, where h is the uniform magnetic field. Then the local-moment action is modified from Eq. (6) by the replacement $\nu \to \nu + imh$ with $m = 0, \pm 1$ denoting the quantum numbers of the three spin-wave modes. By integrating out the local-moment degrees of freedom (i.e., n_q and $\tilde{n}_q$ fields), the free energy for the local moment reads

$$F_{\text{loc}} = \frac{1}{2g}(\eta^2 - h^2)n_0^2$$
$$+ \sum_{m=0,\pm 1}\sum_q \ln[(\nu + imh)^2 + c^2 q^2 + \eta^2]. \quad (49)$$

Then the uniform susceptibility can be obtained from the second-order derivative $\chi_{\text{loc}} = -\partial^2 F_{\text{loc}}/\partial h^2$ taken in the $h \to 0$ limit,

$$\chi_{\text{loc}} = \frac{n_0^2}{g} + 4\sum_q \frac{-\nu^2 + c^2 q^2 + \eta^2}{(\nu^2 + c^2 q^2 + \eta^2)^2}. \quad (50)$$

Carrying out the frequency and momentum summation, we get

$$\chi_{\text{loc}} = \frac{n_0^2}{g} + \frac{1}{\pi\beta c^2}Y\left(\frac{\beta\eta}{2}\right), \quad (51)$$

where the function $Y(x) = x\coth x - \ln(2\sinh x)$.

In the high-temperature limit, according to Eq. (10), the spin-wave mass gap η increases linearly with temperature as $\eta = 2k_B T$, then the function Y tends to a finite limit $Y(1) = 0.458$, resulting in a linear-T behavior

$$\chi_{\text{loc}} = 0.458\frac{k_B T}{\pi c^2}, \quad (52)$$

which will dominate the total uniform susceptibility at high temperature, consistent with the experiments.[42,43]

On the other hand, the itinerant electron uniform susceptibility can be evaluated from

$$\chi_{\text{it}} = -S^2\sum_k \text{Tr}\left[\tau_i G(k)\tau_{i'}G(k)\right], \quad (53)$$

where $S = 1/2$ for the itinerant electrons and the matrix $\tau_i = \sigma_0 \otimes \sigma_i$ represents the spin operator. The particular form of the propagator $G(k)$ will depend on the order in the itinerant electron state. In general, the frequency summation involved can be complicated. However, to the leading order of approximation, we have

$$\chi_{\text{it}} = -\frac{1}{2}\sum_k [n'_F(E_k^+) + n'_F(E_k^-)] + O(n_0^2, \Delta^2), \quad (54)$$

where n'_F is the first-order derivative of the Fermi distribution function and $E_k^{\pm}$ provides the band structure. For normal state, $E_k^{\pm} = \pm\epsilon_k - \mu$, for SDW state, $E_k^{\pm} = \pm(\epsilon_k^2 + J_0^2 n_0^2)^{1/2} - \mu$, and for SC state, $E_k^{\pm} = [(\pm\epsilon_k - \mu)^2 + \Delta^2]^{1/2}$. The remaining terms are of the second-order of the order parameters. Since the function $n'_F(E_k^{\pm})$ peaks at $E_k^{\pm} = 0$, so if the itinerant electron band is gapped from the Fermi surface, the contribution to the uniform susceptibility will decrease rapidly, which accounts for the quick drop of the total uniform susceptibility in the ordered phase in Fig. 6(b).

C. The renormalization of the itinerant electron band

Now we consider the self-energy correction due to the scattering of the itinerant electrons with local moments, which is given by

$$\Sigma_e(k) = -\;\overbrace{}\; = J_0^2\sum_{k'} D_{ii'}(k' - k)s_i G(k')s_{i'}. \quad (55)$$

Here, the local-moment propagator D is taken from Eq. (43) as the RPA-corrected one, while the bare single-particle propagator G is given by Eq. (12) in the normal state and Eq. (18) in the SDW state. The renormalized single-particle propagator obtained from Dyson's equation

$$\tilde{G}(k) = [G(k)^{-1} - \Sigma_e(k)]^{-1} \quad (56)$$

determines the spectral function after a Wick rotation to the real-frequency domain by

$$\tilde{A}(\omega, k) = -2\text{Im}\tilde{G}(\omega + i0_+, k). \quad (57)$$

The result for the hole pocket around the Γ point is shown in Fig. 7. The pocket is slightly more shallow in both the normal and SDW phases, compared to the bare dispersion as indicated by the red dashed curve.

This band renormalization effect can be understood by looking at the frequency dependence of the momentum-
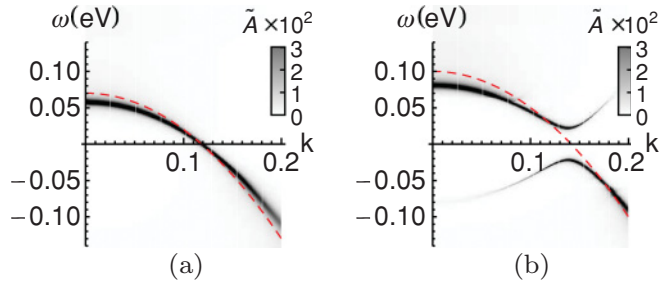
FIG. 7. (Color online) The calculated itinerant electron spectrum for the Γ pocket in (a) the normal phase ($\mu = 0.03$ eV and $T = 70$ K) and (b) the SDW phase ($\mu = 0.00$ eV and $T = 70$ K). Darker shade indicates higher intensity. The red dashed curve marks out the bare dispersion of itinerant electron.

accumulated self-energy $\Sigma_e(\omega) = \sum_k \Sigma_e(\omega, \boldsymbol{k})$, as shown in Fig. 8. The negative imaginary part typically has a valley shape due to the reduced scattering rate within the local-moment gap $\pm \eta$. It can be well approximated by $-2\mathrm{Im}\Sigma_e(\omega + i0_+) \propto \omega^2$ for small frequency ω. According to the Kramers-Kronig relation, the real part of the self-energy should follow $\mathrm{Re}\Sigma_e \propto -\omega$, meaning that the self-energy correction reduces the electron energy above the Fermi level and increases it below the Fermi level, thus always squeezing the electron pockets. This partly accounts for the reduced pocket depth generally observed in ARPES experiments[6–9] compared to the LDA calculations.[11–15]

V. CONCLUSIONS

In this paper, we have presented a systematic study of the itinerant-electron and local-moment hybrid model[46,52] for the iron-based superconductors. The microscopic origin of both the itinerant electron and local-moment degrees of freedom are all from the $3d$ orbitals of the iron atoms. As a renormalization flow at low energy, part of the $3d$ electrons is conjectured to form local moments through an orbital-selective Mott transition. Here, as a simplification, a two-pocket band structure is adopted for the itinerant electrons without considering their Coulomb interaction. A robust short-ranged AF fluctuation around the momentum $\boldsymbol{Q}_s$ is incorporated for the local-moment part via a nonlinear σ description tuned in a disordered regime, which can persist up
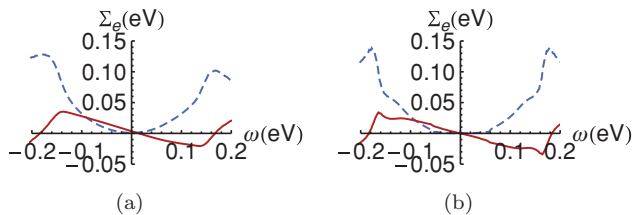

FIG. 8. (Color online) The momentum-accumulated self-energy $\Sigma_e(\omega)$ in (a) the normal phase ($\mu = 0.03$ eV and $T = 70$ K) and (b) the SDW phase ($\mu = 0.00$ eV and $T = 70$ K). The red solid curve represents the real part $\mathrm{Re}(\Sigma_e)$, while the blue dashed curve represents the negative imaginary part $-2\mathrm{Im}(\Sigma_e)$.

to high temperature in the normal state. Thus, in this minimal model, an SDW/AF instability in either subsystem is not intrinsically present when they are decoupled. A Hund's rule ferromagnetic interaction then couples these two subsystems together.

What we have established in this work is that such a simple model is generically infrared unstable against either magnetic or SC ordering at low doping, thanks to the "resonant" scattering of the itinerant electrons between the hole-electron pockets by the local AF fluctuations of the local moments around $\boldsymbol{Q}_s$. In other words, the itinerant electrons form an SDW/SC order by a strong coupling to a background AF fluctuations of the preformed local moments with a momentum match. The phase diagram in Fig. 3 is qualitatively in agreement with the experimental ones in which the Cooper pairing is not glued by the Fermi-surface-nesting-driven collective fluctuations of the itinerant electrons, which would otherwise result in a much weaker pairing strength in a much narrower doping regime close to the SDW phase than what has been shown in Fig. 3. The effective glue provided by the magnetic fluctuations of the local moment automatically favors the $s^{\pm}$-wave paring symmetry here. The presence of the local moments further explains the high-temperature linear-T dependence of the uniform magnetic susceptibility (Fig. 6) in the normal state. In particular, the strong scattering between the itinerant and localized electrons is represented by the dynamic spin susceptibility shown in Fig. 5, which illustrates how the Goldstone mode in the SDW state becomes a resonant-like mode in the SC state as well as its evolution in the normal state. The strong signature of the itinerant/localized electron coexistent picture seen in Fig. 5, including both low- and high-energy parts, can serve as a very useful qualitative prediction for the neutron-scattering measurement even if the comparison may not yet be quantitative due to the highly simplified nature of the model.

Therefore, the minimal model studied in this paper may be generally used to describe the low-energy physics in a multiband electron system in which the electrons in some more localized orbitals may first form short-ranged (fluctuating) SDW order at a higher characteristic temperature (called the hidden local SDW order in Ref. 33). Then at lower temperatures, the electrons in more itinerant orbitals can be naturally driven into a true SDW order or SC state via the Hund's coupling to such a preformed local SDW background. In contrast to the scenario[58] that an electron may carry both a coherent itinerant and an incoherent local-moment signatures, in analog to a single-band case at an intermediate coupling, the multiband case provides us with an alternative but simpler possibility, i.e., via the orbital-selective Mott transition, itinerant and localized electrons may be explicitly separated as independent degrees of freedom.

[1] Y. Kamihara, T. Watanabe, M. Hirano, and H. Hosono, J. Am. Chem. Soc. **130**, 3296 (2008).

[2] H.-H. Wen *et al.*, Europhys. Lett. **82**, 17009 (2008); X. H. Chen *et al.*, Nature (London) **453**, 761 (2008); G. F. Chen, Z. Li, D. Wu, G. Li, W. Z. Hu, J. Dong, P. Zheng, J. L. Luo, and N. L. Wang, Phys. Rev. Lett. **100**, 247002 (2008); Z. A. Ren *et al.*, Europhys. Lett. **83**, 17002 (2008).

[3] J. Paglione and R. L. Greene, Nat. Phys. **6**, 645 (2010).

[4] L. Boeri, O. V. Dolgov, and A. A. Golubov, Phys. Rev. Lett. **101**, 026403 (2008).

[5] C. de. la. Cruz, Q. Huang, J. W. Lynn, J. Li, W. Ratcliff II, J. L. Zarestky, H. A. Mook, G. F. Chen, J. L. Luo, N. L. Wang, and P. Dai, Nature (London) **453**, 899 (2008).

[6] D. H. Lu, M. Yi, S. K. Mo, A. S. Erickson, J. Analytis, J. H. Chu, D. J. Singh, Z. Hussain, T. H. Geballe, I. R. Fisher, and Z. X. Shen, Nature (London) **455**, 81 (2008).

[7] C. Liu, G. D. Samolyuk, Y. Lee, N. Ni, T. Kondo, A. F. Santander Syro, S. L. Bud'ko, J. L. McChesney, E. Rotenberg, T. Valla, A. V. Fedorov, P. C. Canfield, B. N. Harmon, and A. Kaminski, Phys. Rev. Lett. **101**, 177005 (2008).

[8] L. X. Yang, Y. Zhang, H. W. Ou, J. F. Zhao, D. W. Shen, B. Zhou, J. Wei, F. Chen, M. Xu, C. He, Y. Chen, Z. D. Wang, X. F. Wang, T. Wu, G. Wu, X. H. Chen, M. Arita, K. Shimada, M. Taniguchi, Z. Y. Lu, T. Xiang, and D. L. Feng, Phys. Rev. Lett. **102**, 107002 (2009).

[9] G. Liu, H. Liu, L. Zhao, W. Zhang, X. Jia, J. Meng, X. Dong, J. Zhang, G. F. Chen, G. Wang, Y. Zhou, Y. Zhu, X. Wang, Z. Xu, C. Chen, and X. J. Zhou, Phys. Rev. B **80**, 134519 (2009).

[10] T. Sato, K. Nakayama, Y. Sekiba, P. Richard, Y.-M. Xu, S. Souma, T. Takahashi, G. F. Chen, J. L. Luo, N. L. Wang, and H. Ding, Phys. Rev. Lett. **10**, 047002 (2009).

[11] I. I. Mazin, D. J. Singh, M. D. Johannes, and M. H. Du, Phys. Rev. Lett. **101**, 057003 (2008).

[12] K. Kuroki, S. Onari, R. Arita, H. Usui, Y. Tanaka, H. Kontani, and H. Aoki, Phys. Rev. Lett. **101**, 087004 (2008).

[13] D. J. Singh and M. H. Du, Phys. Rev. Lett. **100**, 237003 (2008).

[14] G. Xu, W. Ming, Y. Yao, X. Dai, and Z. Fang, Europhys. Lett. **82**, 67002 (2008).

[15] C. Cao, P. J. Hirschfeld, and H.-P. Cheng, Phys. Rev. B **77**, 220506(R) (2008).

[16] S. E. Sebastian, J. Gillett, N. Harrison, P. H. C. Lau, C. H. Mielke, and G. G. Lonzarich, J. Phys. Condens. Matter **20**, 422203 (2008).

[17] M. Tropeano, C. Fanciulli, C. Ferdeghini, D. Marre', A. S. Siri, M. Putti, A. Martinelli, M. Ferretti, A. Palenzona, M. R. Cimberle, C. Mirri, S. Lupi, R. Sopracase, P. Calvani, and A. Perucchi, Supercond. Sci. Technol. **22**, 034004 (2009).

[18] W. Z. Hu, J. Dong, G. Li, Z. Li, P. Zheng, G. F. Chen, J. L. Luo, and N. L. Wang, Phys. Rev. Lett. **101**, 257005 (2008).

[19] J. Dong, H. J. Zhang, G. Xu, Z. Li, G. Li, W. Z. Hu, D. Wu, G. F. Chen, X. Dai, J. L. Luo, Z. Fang, and N. L. Wang, Europhys. Lett. **83**, 27006 (2008).

[20] K. Kuroki, H. Usui, S. Onari, R. Arita, and H. Aoki, Phys. Rev. B **79**, 224511 (2009).

[21] S. Graser, T. A. Maier, P. J. Hirschfeld, and D. J. Scalapino, New J. Phys. **11**, 025016 (2009); T. A. Maier, S. Graser, D. J. Scalapino, and P. J. Hirschfeld, Phys. Rev. B **79**, 224510 (2009).

[22] Z. J. Yao, J. X. Li, and Z. D. Wang, New J. Phys. **11**, 025009 (2009).

[23] H. Ikeda, J. Phys. Soc. Jpn. **77**, 123707 (2008).

[24] A. V. Chubukov, D. V. Efremov, and I. Eremin, Phys. Rev. B **78**, 134512 (2008); A. V. Chubukov, M. G. Vavilov, and A. B. Vorontsov, *ibid*. **80**, 140515(R) (2009).

[25] F. Wang, H. Zhai, Y. Ran, A. Vishwanath, and D. H. Lee, Phys. Rev. Lett. **102**, 047005 (2009).

[26] F. Wang, H. Zhai, and D.-H. Lee, Phys. Rev. B **81**, 184512 (2010).

[27] R. Thomale, C. Platt, J. Hu, C. Honerkamp, and B. A. Bernevig, Phys. Rev. B **80**, 180505(R) (2009).

[28] F. Yang, H. Zhai, F. Wang, and D. H. Lee, Phys. Rev. B **83**, 134502 (2011).

[29] T. Yildirim, Phys. Rev. Lett. **101**, 057010 (2008).

[30] Q. Si and E. Abrahams, Phys. Rev. Lett. **101**, 076401 (2008).

[31] C. Fang, H. Yao, W.-F. Tsai, J. P. Hu, and S. A. Kivelson, Phys. Rev. B **77**, 224509 (2008).

[32] C. Xu, M. Müller, and S. Sachdev, Phys. Rev. B **78**, 020501(R) (2008).

[33] Z. Y. Weng, Physica E **41**, 1281 (2009).

[34] J. Zhao, D. T. Adroja, D. X. Yao, R. Bewley, S. Li, X. F. Wang, G. Wu, X. H. Chen, J. P. Hu, and P. C. Dai, Nat. Phys. **5**, 555 (2009).

[35] B. Schmidt, M. Siahatgar, and P. Thalmeier, Phys. Rev. B **81**, 165101 (2010).

[36] K. Seo, B. A. Bernevig, and J. Hu, Phys. Rev. Lett. **101**, 206404 (2008).

[37] I. I. Mazin, M. D. Johannes, L. Boeri, K. Koepernik, and D. J. Singh, Phys. Rev. B **78**, 085104 (2008).

[38] H. S. Jeevan, Z. Hossain, D. Kasinathan, H. Rosner, C. Geibel, and P. Gegenwart, Phys. Rev. B **78**, 052502 (2008).

[39] F. Ma, Z. Y. Lu, and T. Xiang, Phys. Rev. B **78**, 224517 (2008).

[40] M. D. Johannes and I. I. Mazin, Phys. Rev. B **79**, 220510(R) (2009).

[41] M. J. Han, Q. Yin, W. E. Pickett, and S. Y. Savrasov, Phys. Rev. Lett. **102**, 107003 (2009).

[42] X. F. Wang, T. Wu, G. Wu, H. Chen, Y. L. Xie, J. J. Ying, Y. J. Yan, R. H. Liu, and X. H. Chen, Phys. Rev. Lett. **102**, 117005 (2009).

[43] R. Klingeler, N. Leps, I. Hellmann, A. Popa, U. Stockert, C. Hess, V. Kataev, H. J. Grafe, F. Hammerath, G. Lang, S. Wurmehl, G. Behr, L. Harnagea, S. Singh, and B. Buchner, Phys. Rev. B **81**, 024506 (2010).

[44] G. M. Zhang, Y. H. Su, Z. Y. Lu, Z. Y. Weng, D. H. Lee, and T. Xiang, Europhys. Lett. **86**, 37006 (2009).

[45] Z. Xu, J. Wen, G. Xu, S. Chi, W. Ku, G. Gu, and J. M. Tranquada, e-print arXiv:1012.2300 (unpublished).

[46] S. P. Kou, T. Li, and Z. Y. Weng, Europhys. Lett. **88**, 17010 (2009).

[47] J. Wu, P. Phillips, and A. H. Castro Neto, Phys. Rev. Lett. **101**, 126401 (2008).

[48] see, M. Vojta, J. Low Temp. Phys. **161**, 203 (2010).

[49] L. de' Medici, Phys. Rev. B **83**, 205112 (2011); L. de' Medici, S. R. Hassan, and M. Capone, J. Supercond. N. Mag. **22**, 535 (2009).

[50] A. Hackl and M. Vojta, New J. Phys. **11**, 055064 (2009).

[51] H. Lee, Y.-Z. Zhang, H. Jeschke, and R. Valenti, Phys. Rev. B **81**, 220506 (2010).

[52]F. Yang, S. P. Kou, and Z. Y. Weng, Phys. Rev. B **81**, 245130 (2010)

[53]W. Lv, F. Krüger, and P. Phillips, Phys. Rev. B **82**, 045125 (2010).

[54]Ying Ran, Fa Wang, Hui Zhai, Ashvin Vishwanath, and Dung-Hai Lee, Phys. Rev. B **79**, 014505 (2009).

[55]J. R. Schrieffer, *Theory of Superconductivity* (Benjamin, New York, 1964); L. P. Gor'kov, Sov. Phys. JETP **9**, 1364 (1959).

[56]A. B. Vorontsov, M. G. Vavilov, and A. V. Chubukov, Phys. Rev. B **79**, 060508 (2009).

[57]M. Ishikado *et al.*, Physica C (2011), doi:10.1016/j.physc. 2011.05.015.

[58]Q. Si, E. Abrahams, J. Dai, and J. X. Zhu, New J. Phys. **11**, 045001 (2009); J. Dai, Q. Si, J. X. Zhu, and E. Abrahams, Proc. Natl. Acad. Sci. USA **106**, 4118 (2009).